RSC Advances

RSC Advances

www.rsc.org/advances

ROYAL SOCIETY OF CHEMISTRY

www.rsc.org/advances

A High-Capacity Dual-Electrolyte Aluminum/Air Electrochemical Cell

Lei Wang,[a] Fude Liu,[a]* Wentao Wang,[a] Guandong Yang,[a] Dawei Zheng,[a] Zhuangchun Wu[b] and

Michael K.H. Leung[c]

[a]Department of Mechanical Engineering, The University of Hong Kong, Hong Kong, China

[b]School of Materials Science and Engineering, Nanjing University of Science and Technology,

Nanjing 210094, China

[c]Ability R&D Energy Research Centre, School of Energy and Environment, City University of

Hong Kong, Hong Kong, China

*Corresponding author: Fude Liu; Electronic mail: fordliu@hku.hk; Department of Mechanical

Engineering, The University of Hong Kong, Pokfulam Road, Hong Kong; phone: (+852) 2859

2631; FAX: (+852) 2858-5415

Abstract

A novel dual-electrolyte aluminum/air cell (DEAAC), consisting of an aluminum metal anode in an organic anolyte, an anion polymer exchange membrane, and an air electrode in an aqueous alkaline catholyte, has been investigated. The anion membrane separates the organic anolyte from the aqueous catholyte, while allowing hydroxide ions to pass through. The DEAAC exhibited an open circuit voltage (V_{OC}) of 1.6 V and a short current density (J_{SC}) of 65 mA cm^{-2}. With kitchen aluminum foil as the fuel, the DEAAC achieved an anodic capacity of 6000 mAh cm^{-3} at a discharge current density of 30 mA cm^{-2}, which is much higher than the lithium's theoretical capacity of 2060 mAh cm^{-3}. The anodic capacity of the DEAAC increased by 30−50 folds at different discharge current densities compared with that of a traditional alkaline Al/air cell (AAC). Overall, the DEAAC is promising as an electrochemical energy storage device because it has no detrimental hydrogen generation problem and exhibits very high anodic capacity.

Keywords: energy storage; aluminum/air battery; dual-electrolyte fuel cell; organic electrolyte; parasitic reaction.
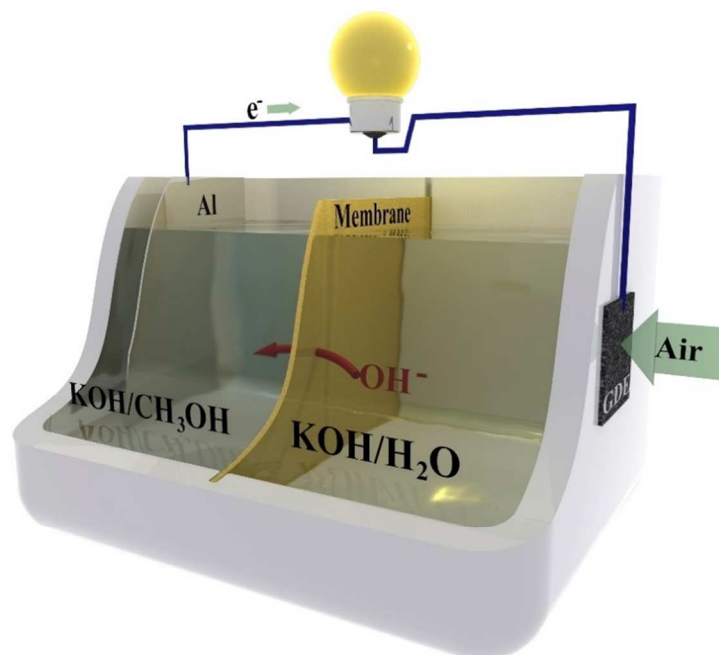
1. Introduction

To realize a sustainable modern society, batteries have seen ever demanding challenges in diverse applications ranging from portable electronics and electrical vehicles to grid-level energy storage.[1-4] Metal/air electrochemical cells lie at the intersection of classical battery design and modern fuel cell concept while combining advantages of both.[5] With a reactive anode coupled with an air-breathing cathode, a metal/air cell takes in oxygen from the inexhaustible air and, in some cases, exhibits very high gravimetric and volumetric energy density.[6] Among various metal candidates such as lithium, magnesium, calcium, zinc and iron, aluminum has been considered as a highly promising energy carrier, given its earth abundance, low price, environmental benignity, high capacity and energy density, and strong recyclability.[7-10] The theoretical volumetric capacity of aluminum (8046 mAh cm^{-3}) is approximately four times higher than that of lithium (2062 mAh cm^{-3}), which makes it more attractive for small portable electronics. Although the lithium/air cell possesses the highest theoretical energy density, it is still in the early laboratory development and most reported studies utilize pure oxygen rather than air as the oxidant to prevent possible parasitic reactions.[11] Sodium has been explored as an alternative to the costly and scarce lithium but with compromised capacity and energy density.[12-14] Recently, Duan's group has broadened the classical metal/air concept to the metalloids and demonstrated high capacity silicon/air and alkaline silicide/air batteries.[15, 16] Yet these cells exhibit low discharge current densities ($\leq$ 1 mA cm^{-2}) at normal operation voltages due to the poor conductivity and reactivity of Si and silicide in alkaline. Moreover, these cells still have the anodic self-corrosion problem as in typical alkaline metal/air batteries.

Research on Al/air cells has spanned over fifty years since the 1960s and their applications have been limited to niche markets so far.[17] The anodic self-corrosion problem is the major

challenge faced by traditional Al/air batteries, which increases the hydrogen explosion possibility and causes unacceptably high energy losses.[7, 8] Researchers have attempted to inhibit the hydrogen generation reaction by alloying aluminum with other elements[7, 18, 19] or modifying the electrolyte using certain additives.[20-22] However, these efforts have shown limited success, and oftentimes have increased the material cost and complexity of the battery system. Recently, we demonstrated a hybrid $Al/H_2/air$ cell system to turn the parasitic hydrogen-evolution reaction into a beneficial process through hydrogen utilization.[23] However, to really solve the hydrogen evolution problem, aluminum oxidation should take place in a nonaqueous environment with high aluminum anode activity whilst reducing the corrosion rate to a low level.[24] Licht *et al.* conducted a series of studies on the electrochemical behavior of aluminum in organic electrolytes and achieved improved aluminum coulombic efficiency.[25-28] Other approaches, including employing gel electrolytes, membranes or ionic liquids, have also been proposed to tackle the self-corrosion problem.[17, 29] Herein we developed a novel dual-electrolyte Al/air cell (DEAAC) with a structure of Al anode | organic electrolyte || anion exchange membrane || aqueous electrolyte | air cathode. In the DEAAC, a nonaqueous anolyte and an aqueous catholyte are separated by an anion exchange membrane so that the aluminum oxidation reaction occurs in an organic-solvent-based alkaline environment. The hydrogen evolution reaction is thus suppressed to a minimal level and a very high cell capacity is achieved. In addition, the dual-electrolyte configuration provides more flexibility in choosing anolyte and catholyte. This primary cell can also be mechanically recharged by replenishing the aluminum anode.

2. Experimental

2.1 Experimental setup

(1) Cell construction. As shown in Fig. 1a, a traditional Al/air cell (AAC) with an aqueous alkaline electrolyte was set up as the benchmark for performance comparison. The DEAAC (Fig. 1b) was designed and fabricated with SolidWorks® and 3D rapid prototyping technologies using an alkaline resistant polymer, respectively. The two chambers of the DEAAC were assembled with a membrane in between and fastened by bolts.

(2) Anode. As a cost-effective fuel source, ordinary kitchen aluminum foil (~16.2 μm thick) rather than expensive specially formulated alloys or high-purity aluminum was employed as the anode. The foil composition was studied with scanning-electron-microscopy energy-dispersive X-ray (SEM/EDX) analyses and the results showed a uniform Al purity of 97.60 wt% (impurities: O 1.13 wt%, Fe 0.68 wt%, and Ag 0.59 wt%). The foil was cut and integrated into an electrode fixture with an effective area of 3×4 cm^2 (effective Al weight of 52.5 mg) exposed to anolyte.

(3) Membrane. The two chambers of DEAAC were separated by a strong alkali anion exchange membrane (450 μm thick; AMI7001; Membrane International Inc., USA). The active area of the membrane is 30 cm^2 and the predicted electrical resistance is < 40 Ω·cm^2 in a 0.5 M NaCl solution. The membrane was pre-treated in a 5 wt% NaCl solution at 40°C for 24 hours to allow for membrane hydration and expansion.

(4) Cathode. Gas diffusion electrode (GDE) (120 μm thick) with catalyst loading of 2 mg cm^{-2} 60% Pt-C (Johnson Matthey Catalysts, UK) was used as the air-breathing cathode. The effective cathode area of 1 cm^2 was used to calculate the current and power densities.

(5) Electrolyte. For the traditional AAC, the electrolyte was a 3 M potassium hydroxide aqueous solution (KOH/H_2O). For the DEAAC, the organic anolyte was 3 M KOH in anhydrous methanol solvent (KOH/CH_3OH) and the aqueous catholyte was a 3 M potassium hydroxide solution (KOH/H_2O). For both cells, electrolytes were purged with nitrogen for over ten minutes before use.

Fig. 1
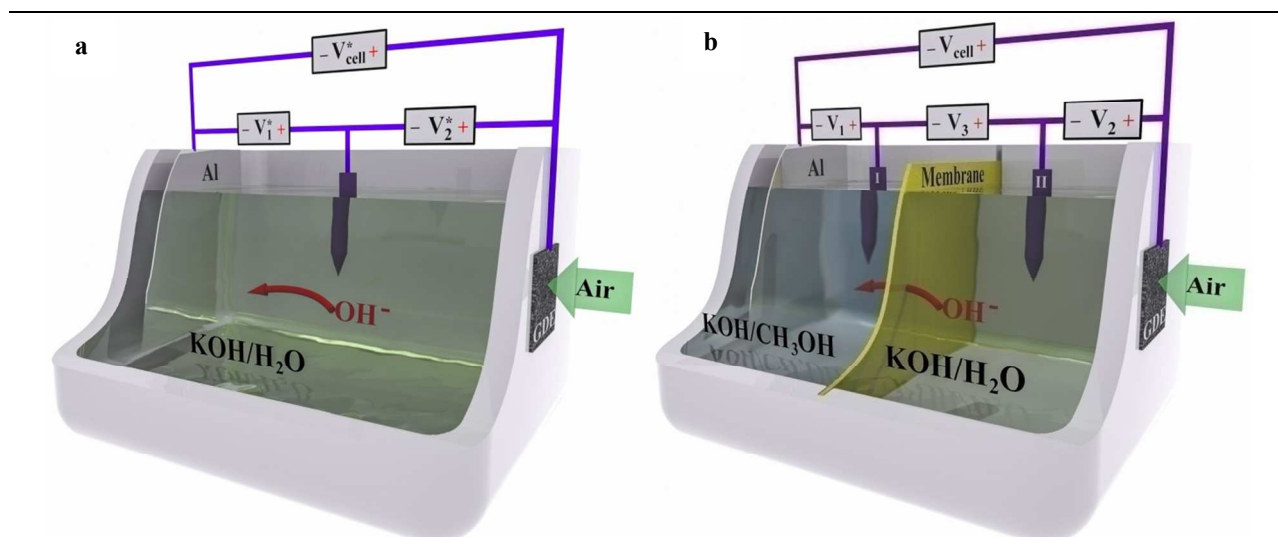
Fig. 1 Schematics and experimental setups of two cells (not drawn to scale). **(a)** Traditional AAC. **(b)** DEAAC.

2.2 Electrochemical tests

For testing the traditional AAC (Fig. 1a), a three-electrode configuration was used by placing a reference electrode (Hg/HgO/1 M NaOH; 0.14 V *vs.* SHE at 25°C) into the electrolyte. For the DEAAC (Fig. 1b), a four-electrode configuration was used by inserting one Hg/HgO reference electrode in the anolyte and the other one in the catholyte. Excess electrolyte (60 mL
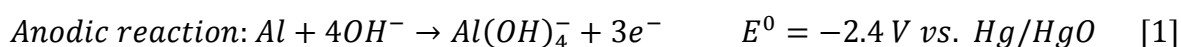
aqueous electrolyte for the AAC; 30 mL anolyte and 30 mL catholyte for the DEAAC) was injected into the cell to minimize the concentration change due to cell reactions and carbonate formation related to atmospheric carbon dioxide. The DEAAC was left idle for twenty minutes to reach ionic balance across the membrane before inserting the aluminum anode. Aluminum was inserted into the cell immediately before use to avoid self-corrosion under stand-by condition. The current-voltage polarization curves were acquired with steady-state potentiostatic techniques using an electrochemical station (Reference 3000™, Gamry Instruments). The cell potential was stepped from 0 V to the open circuit voltage (V_{OC}) by a 0.2 V increment with each discharge current recorded over three minutes until steady state conditions were reached. The average value of the current data (I-t) was used to represent the cell current at a certain voltage. The anodic polarization, cathodic polarization, and potential drop across membrane were simultaneously recorded *in situ*, as shown in Figs. 1a and 1b. The voltage across each individual component was monitored and recorded with digital multimeters (Agilent 34401A). For the AAC, $V_1^*(= \phi_{Al} - \phi_{RE})$ is the potential difference between the Al anode and Hg/HgO reference electrode; $V_2^*(= \phi_{GDE} - \phi_{RE})$ is the potential difference between the air cathode (GDE) and Hg/HgO reference electrode; $V_{cell}^*(= \phi_{GDE} - \phi_{Al} = V_2^* - V_1^*)$ is the potential difference between the cathode and anode or the cell voltage. For the DEAAC, $V_1(= \phi_{Al} - \phi_{RE1})$ is the potential difference between the Al anode and Hg/HgO reference electrode I; $V_2(= \phi_{GDE} - \phi_{RE2})$ is the potential difference between the air cathode (GDE) and Hg/HgO reference electrode II; $V_3(= \phi_{RE1} - \phi_{RE2})$ is the potential difference between the two reference electrodes I and II across the anion membrane, i.e., the membrane overpotential; $V_{cell}(= \phi_{GDE} - \phi_{Al} = V_2 - V_1 - V_3)$ is the cell voltage. Each cell capacity was evaluated by galvanostatically discharging the full cell using a two-electrode setup until the aluminum foil was totally consumed and the cell ceased

functioning. All tests were conducted under standard ambient temperature and pressure (25°C and 1 atm).

3. Results and discussion

3.1 Polarization and power characteristics

The anodic and cathodic reactions in an Al/air cell are shown as follows:[17]

$$Anodic\ reaction: Al + 4OH^- \rightarrow Al(OH)_4^- + 3e^- \qquad E^0 = -2.4\ V\ vs.\ Hg/HgO \quad [1]$$

$$Cathodic\ reaction: O_2 + 2H_2O + 4e^- \rightarrow 4OH^- \qquad E^0 = 0.3\ V\ vs.\ Hg/HgO \qquad [2]$$

In aqueous media, aluminum will also be consumed through a parasitic reaction to generate hydrogen:

$$Parasitic\ reaction: 2Al + 6H_2O + 2OH^- \rightarrow 2Al(OH)_4^- + 3H_2 \uparrow \qquad [3]$$
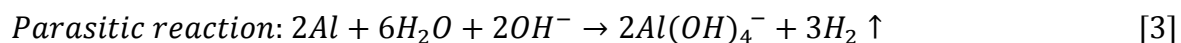
As shown in Fig. 2a, the benchmark AAC exhibits a linear polarization curve with a V_{OC} of 1.5 V, a short-circuit current density (J_{SC}) of 241 mA cm^{-2}, and an internal resistance of 6.2 $\Omega \cdot cm^2$ ($= \Delta V/\Delta J = 1.5$ V $\div$ 241 mA cm^{-2}). The maximum power density reaches 85 mW cm^{-2} at 107 mA cm^{-2}. In comparison, the DEAAC has a slightly higher V_{OC} of 1.58 V but lower J_{SC} of 65 mA cm^{-2} and peak power density of 28 mW cm^{-2} (Fig. 2b). In addition, the DEAAC has a higher internal resistance of 24.3 $\Omega \cdot cm^2$ ($= 1.58$ V $\div$ 65 mA cm^{-2}), because of the less-conductive organic electrolyte and increased ionic resistance across the anion membrane.

Fig. 2
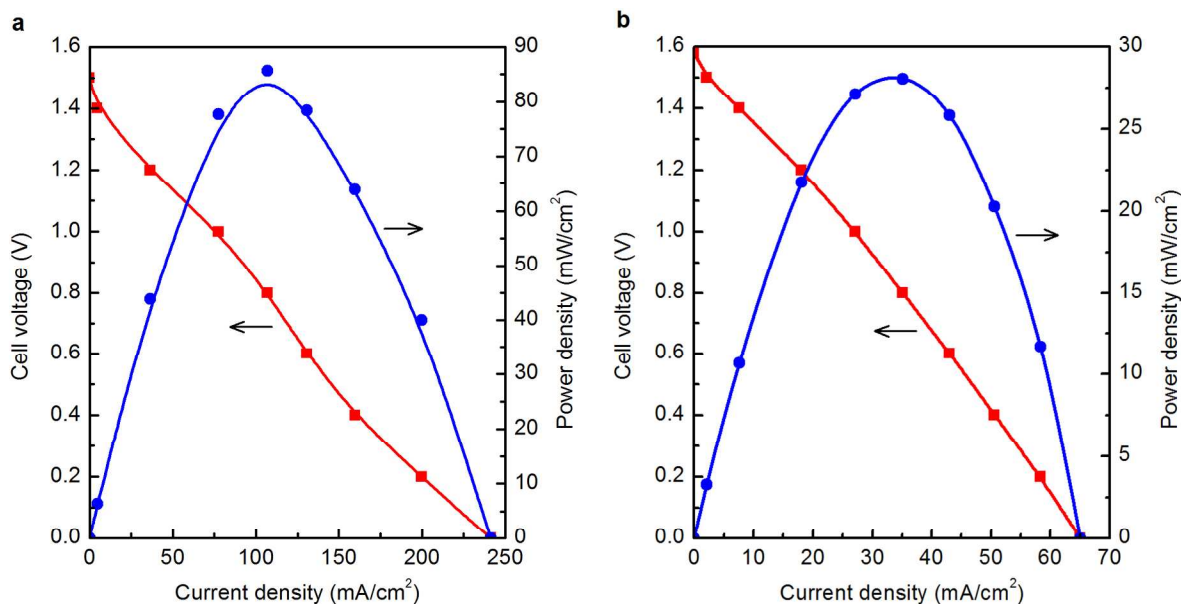
Fig. 2 Polarization curves and power density plots. **(a)** Traditional AAC. **(b)** DEAAC.

In situ single electrode characterization techniques were adopted to study each component of the cells by properly placing Hg/HgO reference electrode(s) into the electrolyte, and the results are shown in Fig. 3. For the AAC (Fig. 3a), both anode and cathode experienced a linear voltage drop with current increase, indicating that electrochemical reactions on both electrodes are dominated by ohmic losses. Over the entire current range, the cathode voltage (V_2^*) dropped significantly by 1.21 V from 0.06 to -1.15 V, contributing to four-fifth of the overall cell voltage drop with a corresponding ohmic resistance of 5.0 $\Omega \cdot cm^2$ ($= \Delta V_2^*/\Delta J = 1.21$ V $\div$ 241 mA cm^{-2}). In contrast, the anode voltage (V_1^*) changed slightly by 0.29 V from -1.44 to -1.15 V, corresponding to an ohmic resistance of 1.2 $\Omega \cdot cm^2$ ($= 0.29$ V $\div$ 241 mA cm^{-2}). The aluminum

anode exhibited, however, a substantial activation loss of ~1.0 V, considering the aluminum's open circuit potential of -1.44 V and its theoretical potential of -2.4 V. This activation loss is mainly due to the parasitic reaction and the resultant mixed-potential.[23] Overall for the AAC, its V_{OC} is mainly limited by the anodic activation loss and its J_{SC} by the cathodic ohmic loss.

Fig. 3
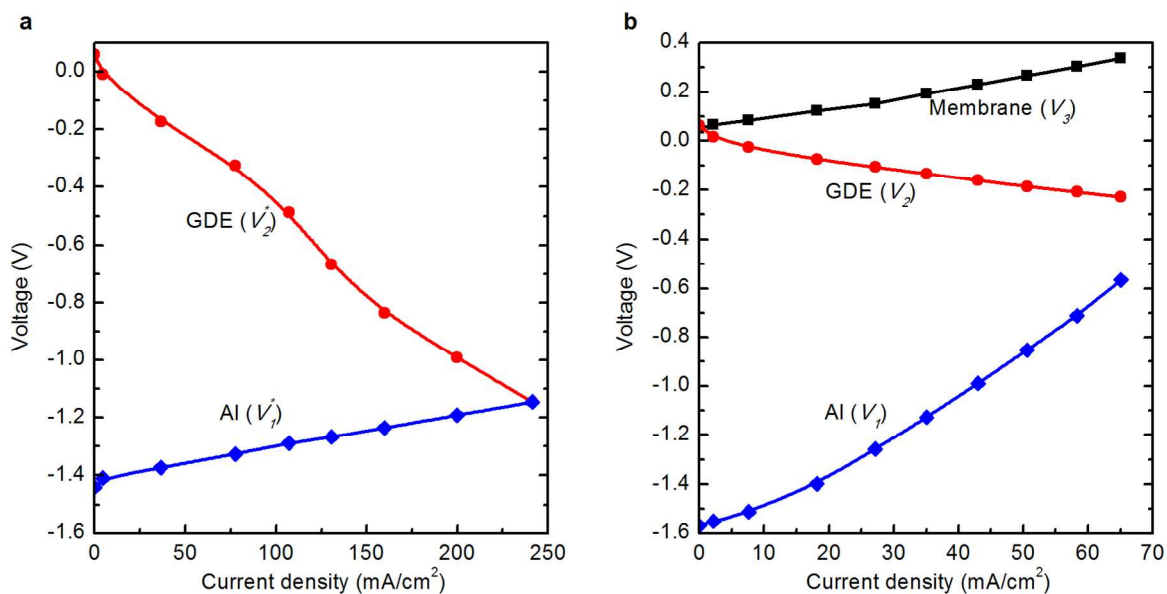
Fig. 3 Single-electrode polarization curves. **(a)** Traditional AAC. **(b)** DEAAC. Also included is the membrane polarization curve (J-V_3).

For the DEAAC case (Fig. 3b), besides potential drops at the anode (V_1) and cathode (V_2), there is also a potential drop across membrane (V_3), which is related to both chemical and electrostatic potentials that drive hydroxide ions to flow through.[30, 31] The aluminum anode in the

DEAAC exhibits a slightly higher open circuit potential of -1.57 V than that in the AAC, but its ohmic overpotential (from -1.57 to -0.57 V) plays a dominant role for the overall cell voltage drop, as opposed to the AAC case (from -1.44 to -1.15 V). V_1, V_2 and V_3 contribute a voltage drop of 1.0, 0.292 and 0.286 V, respectively, over the entire current range. The anodic ohmic resistance of the DEAAC is 15.4 $\Omega \cdot cm^2$ (= 1.0 V ÷ 65 mA cm^{-2}) (in contrast, the value for the AAC is 1.2 $\Omega \cdot cm^2$), contributing nearly three-fifth to the overall internal resistance (24.3 $\Omega \cdot cm^2$). As expected, the cathodic ohmic resistance is 4.5 $\Omega \cdot cm^2$ (= 0.292 V ÷ 65 mA cm^{-2}), similar to the AAC case. Interestingly, the membrane exhibits a satisfactory ionic conductivity of 4.4 $\Omega \cdot cm^2$ (= 0.286 V ÷ 65 mA cm^{-2}) so that the membrane overpotential can be relatively small. In fact, by further reducing the membrane thickness (450 μm) to the level of Nafion membranes (50–175 μm), an even lower overpotential V_3 and thus better cell performance can be attained. Therefore, the low current and power densities of the DEAAC, compared with the AAC case, were mainly resulted from aluminum's lower electrochemical activity in the organic electrolyte than in the aqueous media[25] and the associated higher anodic ohmic loss. Similar dual-electrolyte configuration has been adopted in a Li/air battery.[32, 33] However, the high internal resistance of the solid lithium-ion conducting electrolyte seriously impairs the conversion efficiency and power density of dual-electrolyte Li/air cells.[34]

3.2 Discharge characteristics

The discharge curves of traditional AAC (Fig. 4a) and DEAAC (Fig. 4b) reveal that aluminum can exhibit much more efficient coulombic oxidation in organic electrolytes than in aqueous ones, which is in consistent with findings by Licht *et al*.[25, 26] In fact, the hydrogen generation was barely observed in the DEAAC, indicating that the parasitic reaction was almost

completely suppressed. Wang *et al.*[24] have reported a similar phenomenon that the self-corrosion rate of aluminum in KOH/CH_3OH solutions is less than 5% of that in KOH/H_2O solutions. Both AAC and DEAAC can maintain flat voltage plateaus, which is consistent with the polarization results in Fig. 2. At a discharge current density of 10 mA cm^{-2}, the AAC achieved a capacity of 89 mAh cm^{-3} (Fig. 4a), which is only ~1.1% of aluminum's theoretical capacity. In contrast, the DEAAC exhibited a much superior capacity of 4310 mAh cm^{-3} at the same current density (see the red curve in Fig. 4b), which is ~53.6% of the theoretical value. At 20 and 30 mA cm^{-2}, the AAC and DEAAC exhibit capacities of 145 and 195 mAh cm^{-3}, and 4881 and 5952 mAh cm^{-3}, respectively. Although the AAC exhibited a slightly higher voltage at each discharge current density, its coulombic efficiency reaches only 2.4% at 30 mA cm^{-2}, which is significantly lower than the 74.0% efficiency of the DEAAC achieved at the same current density. Even though operating at a higher current density could help the AAC achieve a higher capacity (~1700 mAh cm^{-3} at 100 mA cm^{-2} and a small voltage of ~0.85 V), its capacity and energy density are still much lower than those of the DEAAC (see Fig. S2 in the Supplementary Materials for details). Compared with the AAC case, the DEAAC's anodic capacity increases by 33 and 31 folds at 20 and 30 mA cm^{-2}, respectively. The extraordinary capacity improvement is the major merit of the dual-electrolyte configuration with organic anolyte. Researchers have investigated the aluminum's electrochemical behaviors in alkaline alcohol solutions and found that it undergoes a similar reaction mechanism as in the aqueous alkaline solution but with the parasitic reaction significantly suppressed.[24, 35, 36] This is consistent with our experimental observation that the self-corrosion rate of aluminum in methanol alkali under open circuit condition is only ~2.5% of that in aqueous alkali (see the Supplementary Materials for details). So it is reasonable that the DEAAC has much higher capacities than the AAC.

With increased discharge current density, Al/air systems (both AAC and DEAAC) achieved higher capacities, as opposed to typical Li-ion batteries whose capacity declines. This is due to the competition between the parasitic reaction (Eqn. [3]) that consumes electrons to generate hydrogen and the main anodic reaction (Eqn. [1]) that releases electrons to the external circuit. When discharged at higher current densities, because the aluminum oxidation rate increases dramatically and the hydrogen generation rate increases slightly, a higher proportion of electrons flow to the external circuit. Therefore the cell exhibits higher coulombic efficiencies and capacities at higher current densities. This is consistent with our previous findings[23] and other reports[35, 37] on the aluminum's electrochemical behavior in organic electrolytes.

Fig. 4
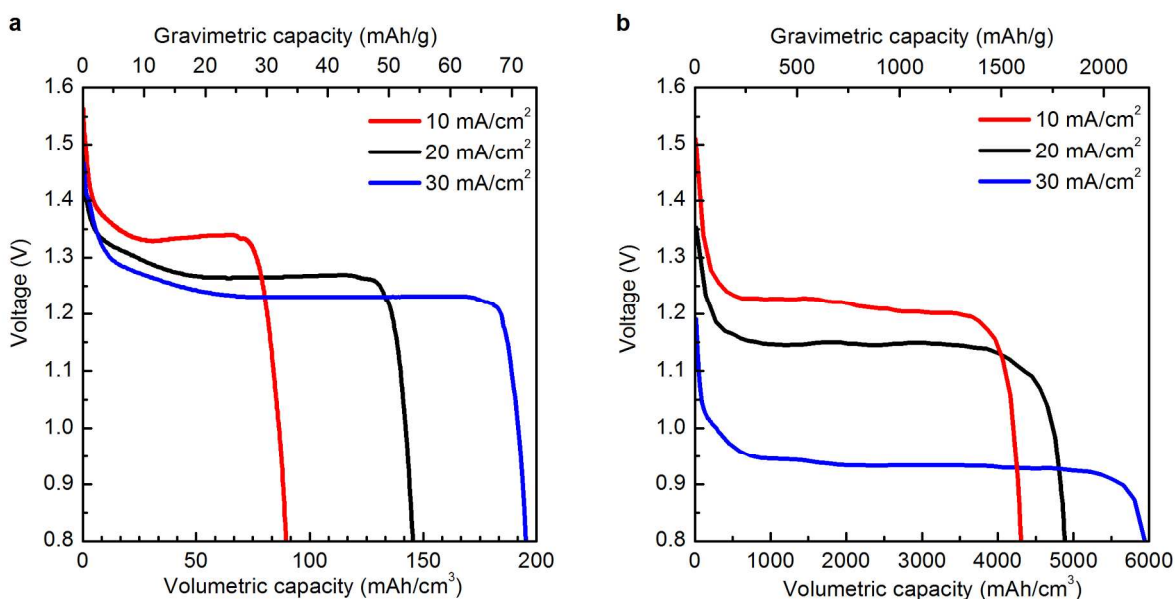
Fig. 4 Typical discharge curves at different current densities. **(a)** Traditional AAC. **(b)** DEAAC.

Throughout the entire discharge process, almost no hydrogen bubbles were observed in the DEAAC while there was a violent hydrogen evolution in the AAC. This further confirms that the high discharge capacity of the DEAAC was due to the suppressed self-discharge reaction in the organic anolyte. We also verified no water or methanol crossover through the membrane with an impermeability test that was conducted by filling one chamber of the DEAAC with corresponding electrolyte while leaving the other one empty; no liquid leakage was found on the dry side of the membrane over 24 hours. A further crossover check was conducted: a droplet of methyl red was added into one chamber to make it yellow, and no yellow color was observed in the other chamber over 48 hours of cell discharge. The absence of crossover can also be confirmed by the discharge curves of the DEAAC shown in Fig. 4b where we see flat voltage plateaus. If there is methanol crossover to the air cathode, a voltage drop will be observed because of the parasitic methanol oxidation reaction on the GDE cathode. If there is water crossover to the anode, a voltage rise will be expected under the galvanostatic discharge since the aluminum has higher reaction rate in the aqueous solution.

3.3 Performance comparison of the DEAAC with other metal/air cells

The performance of the DEAAC was compared with that of reported high-performance metal/air cells (Table 1). The DEAAC has a gravimetric energy density of 2081 Wh kg^{-1}, which is over four folds higher than that of aqueous alkaline Al/air cells (300–500 Wh kg^{-1}) reported in the literature.[8, 38] Saline Al/air cells have lower corrosion rates than alkaline Al/air cells, and can achieve an energy density up to 800 Wh kg^{-1} which is still much lower than that of the DEAAC.

[39] In fact, due to the low solubility of $Al(OH)_3$ in the neutral electrolyte (e.g., 12 wt% sodium chloride solution), a large amount of electrolyte is required to avoid $Al(OH)_3$ precipitation and consequently the system energy density of saline cells could be even lower than that of alkaline cells.[17] With high energy densities, Zinc/air batteries are so far the only commercialized metal/air devices for niche markets, for example, hearing aids. Dai's group[40] in 2013 reported a Zn/air cell that has a gravimetric energy density of 741 Wh kg^{-1} with advanced hybrid electrocatalysts and outperforms most commercially available Zn/air batteries (200–300 Wh kg^{-1}).[38, 41] Compared to Dai's Zn/air cell,[40] the DEAAC exhibits three-fold gravimetric capacity and energy density, and has slightly higher volumetric capacity and energy density. Recently, silicon has emerged as a new anode candidate given its high theoretical capacity (3817 mAh g^{-1} and 8890 mAh cm^{-3}) and energy density (8359 Wh kg^{-1} and 19469 Wh L^{-1}) (see Table S1 in Supplementary Materials).[15, 16, 42-44] Silicon undergoes a similar reaction mechanism as aluminum and zinc in alkaline electrolytes. The DEAAC outperforms the reported high-capacity alkaline Si/air cell[15] in terms of energy density (both gravimetric and volumetric) and discharge current density (10–30 mA cm^{-2} *vs.* 0.01–0.1 mA cm^{-2}); its volumetric capacity (5950 mAh cm^{-3} at 30 mA cm^{-2}) is more than twice as high as that of the Si/air cell (2809 mAh cm^{-3} at 0.1 mA cm^{-2}). As Li-ion batteries are approaching their maximum potential energy density and are unable to meet the long-term needs, researchers have recently paid tremendous efforts to Li/air cells owing to their considerably 3−5 times higher anodic gravimetric energies than Li-ion batteries.[45] Jun *et al.*[46] have developed an improved rechargeable Li/air cell. After detailed calculations (see Supplementary Materials), the cell discharge current density is actually 0.5 mA cm^{-2} at 2.7 V with a limited anodic capacity of 234 mAh cm^{-3} (i.e., 11% of the lithium's theoretical capacity). The results of this Li/air cell are actually consistent with the well-known statement[47] that current densities (0.05–1 mA cm^{-2}) of

Li/air cells so far are too low for most of practical applications. Although this Li/air cell is rechargeable, the DEAAC exhibits at least one order of magnitude higher capacities and energy densities and its anode can be mechanically replaced. Hayashi *et al.*[14] have investigated a mixed aqueous/aprotic Na/air primary cell that has a similar cell structure as the DEAAC (see Table 1). Compared to the DEAAC, the Na/air cell has a higher V_{OC} (2.85 V *vs.* 1.58 V), but exhibits a remarkably lower peak power density (5 mW cm^{-2} *vs.* 28 mW cm^{-2}). While the Na/air cell exhibits a similar gravimetric energy density as the DEAAC, its volumetric energy density and capacity are much lower than those of the DEAAC. The authors attribute the cell's inferior performance to the high internal resistance of ~440 Ω associated mainly with the NASICON ceramic membrane (65 Ω) and the aqueous electrolyte (200 Ω).[14] In contrast, with the highly conductive polymer membrane and high-concentration KOH electrolyte, the DEAAC has a much lower internal resistance of ~24.3 Ω and hence has significantly less power and energy losses. Note that more than enough electrolyte has been used in the DEAAC to make sure that Al(OH)$_3$ will not precipitate. Also, the weight of the electrolyte and the cell case has not been taken into consideration (which will reduce the overall energy density of course). So in our future work the amount of electrolyte will be optimized so that an appropriate evaluation of the overall cell energy density may be achieved.

Table 1 Comparison of DEAAC with reported high-performance metal/air cells[‡]

	DEAAC	Zn/air[40]	Si/air[15]	Li/air[46]	Na/air[14]
Cell structure	(See Fig. 1b)	Zn | 6 M aqueous KOH | O_2	Si nanowire | 0.6 M aqueous KOH | air	Li | TEGDME– $LiCF_3SO_3$ | O_2	Na | organic electrolyte || ceramic membrane || aqueous NaOH | O_2
Discharge voltage (V)	1.15	1.3	0.85	2.7	2.5
Discharge current density (mA cm^{-2})	20	10	0.1	0.5 (500 mA g$^{-1}_{carbon}$)	0.63
Gravimetric capacity (mAh g^{-1})	1810	570	1206	234 (5000 mAh g$^{-1}_{carbon}$)	835
Volumetric capacity (mAh cm^{-3})	4886	4070	2809	125	808
Gravimetric energy density (Wh kg^{-1})	2081	741	1025	631.8	2087
Volumetric energy density (Wh L^{-1})	5819	5291	2387	337	2020

[‡] Capacity and energy density values are based on the anode alone. All data is reported on primary cells expect the Li/air that is rechargeable. Detailed derivations are included in the Supplementary Materials.

With enough electrolytes, the DEAAC could run at the same performance level by simply replenishing the aluminum anode. Recently, an Al/air battery system has been demonstrated to power electric vehicles with driving ranges and acceleration similar to gasoline powered cars.[38, 48] The battery system can be quickly refueled with new aluminum plates and fresh electrolyte. Our DEAAC is suitable for such a mechanically rechargeable battery system. By increasing the aluminum effective area to fully utilize the GDE's current capacity and properly connecting cells into stack, we believe the DEAAC also promises to be a reliable and scalable stationary power backup.

4. Conclusions

In summary, we investigated a novel high-capacity dual-electrolyte Al/air semi-fuel cell with an anion exchange membrane separating the organic anolyte and the aqueous catholyte. The dual-electrolyte structure is a novel approach to solving the parasitic self-corrosion problem in traditional alkaline metal/air batteries. The DEAAC successfully suppressed the parasitic reaction and hence achieved superior anodic capacities compared with traditional alkaline Al/air cells. The measured anode capacity of the DEAAC (6000 mAh cm^{-3} at 30 mA cm^{-2}) is even greater than the lithium's theoretical capacity (2060 mAh cm^{-3}). The DEAAC shows a high energy density of 2081 Wh kg^{-1} (or 5819 Wh L^{-1}). The DEAAC can be mechanically rechargeable and has more flexibility in choosing appropriate anolyte, catholyte and membrane. With all these features, we believe that the DEAAC is a promising electrochemical power source in various applications such as electric vehicles and power backup.

References

1. M. Armand and J. M. Tarascon, *Nature*, 2008, **451**, 652−657.

2. Z. G. Yang, J. L. Zhang, M. C. W. Kintner-Meyer, X. C. Lu, D. W. Choi, J. P. Lemmon and J. Liu, *Chem Rev*, 2011, **111**, 3577−3613.

3. B. Dunn, H. Kamath and J. M. Tarascon, *Science*, 2011, **334**, 928−935.

4. J. B. Goodenough, *Energ Environ Sci*, 2014, **7**, 14−18.

5. M. Winter and R. J. Brodd, *Chem Rev*, 2004, **104**, 4245−4269.

6. T. B. Reddy, *Linden's Handbook of Batteries*, McGraw-Hill, 2011, p. 33.31−33.32.

7. Q. F. Li and N. J. Bjerrum, *J Power Sources*, 2002, **110**, 1−10.

8. E. I. Shkolnikov, A. Z. Zhuk and M. S. Vlaskin, *Renew Sust Energ Rev*, 2011, **15**, 4611−4623.

9. W. Y. Li, C. S. Li, C. Y. Zhou, H. Ma and J. Chen, *Angew Chem Int Edit*, 2006, **45**, 6009−6012.

10. B. T. Hang, T. Watanabe, M. Egashira, I. Watanabe, O. Shigeto and J. Yamaki, *J Power Sources*, 2006, **155**, 461−469.

11. J. S. Lee, S. T. Kim, R. Cao, N. S. Choi, M. Liu, K. T. Lee and J. Cho, *Adv Energy Mater*, 2011, **1**, 34−50.

12. H. Pan, Y.-S. Hu and L. Chen, *Energ Environ Sci*, 2013, **6**, 2338−2360.

13. P. Hartmann, C. L. Bender, M. Vracar, A. K. Durr, A. Garsuch, J. Janek and P. Adelhelm, *Nat Mater*, 2013, **12**, 228−232.

14. K. Hayashi, K. Shima and F. Sugiyama, *J Electrochem Soc*, 2013, **160**, A1467−A1472.

15. X. Zhong, H. Zhang, Y. Liu, J. W. Bai, L. Liao, Y. Huang and X. F. Duan, *Chemsuschem*, 2012, **5**, 177−180.

16.   H. Zhang, X. Zhong, J. C. Shaw, L. Liu, Y. Huang and X. Duan, *Energ Environ Sci*, 2013, **6**, 2621−2625.

17.   D. R. Egan, C. Ponce de León, R. J. K. Wood, R. L. Jones, K. R. Stokes and F. C. Walsh, *J Power Sources*, 2013, **236**, 293−310.

18.   D. Macdonald, K. Lee, A. Moccari and D. Harrington, *Corrosion*, 1988, **44**, 652−657.

19.   M. Doche, F. Novel-Cattin, R. Durand and J. Rameau, *J Power Sources*, 1997, **65**, 197−205.

20.   A. Abdel-Gaber, E. Khamis, H. Abo-ElDahab and S. Adeel, *Mater Chem Phys*, 2008, **109**, 297−305.

21.   O. K. Abiola and J. Otaigbe, *Corrosion Sci*, 2009, **51**, 2790−2793.

22.   T. Hirai, J. Yamaki, T. Okada and A. Yamaji, *Electrochimica Acta*, 1985, **30**, 61−67.

23.   L. Wang, W. Wang, G. Yang, D. Liu, J. Xuan, H. Wang, M. K. H. Leung and F. Liu, *Int J Hydrogen Energ*, 2013, **38**, 14801−14809.

24.   J.-B. Wang, J.-M. Wang, H.-B. Shao, J.-Q. Zhang and C.-N. Cao, *Journal of Appl Electrochem*, 2007, **37**, 753−758.

25.   S. Licht, G. Levitin, C. Yarnitzky and R. Tel-Vered, *Electrochem and Solid St*, 1999, **2**, 262−264.

26.   S. Licht, R. Tel‑Vered, G. Levitin and C. Yarnitzky, *J Electrochem Soc*, 2000, **147**, 496−501.

27.   S. Licht, G. Levitin, R. Tel-Vered and C. Yarnitzky, *Electrochem Commun*, 2000, **2**, 329−333.

28.   G. Levitin, C. Yarnitzky and S. Licht, *Electrochem and Solid St*, 2002, **5**, A160−A163.

29.   Z. Zhang, C. Zuo, Z. Liu, Y. Yu, Y. Zuo and Y. Song, *J Power Sources*, 2013, **251**, 470−475.

30.   V. M. Aguilella, S. Mafe, J. A. Manzanares and J. Pellicer, *J Membrane Sci*, 1991, **61**, 177−190.

31.   E. Volodina, N. Pismenskaya, V. Nikonenko, C. Larchet and G. Pourcelly, *J of Colloid Interf Sci*, 2005, **285**, 247−258.

32.   L. J. Li, X. S. Zhao and A. Manthiram, *Electrochem Commun*, 2012, **14**, 78−81.

33.   J. P. Zheng, P. Andrei, M. Hendrickson and E. J. Plichta, *J Electrochem Soc*, 2011, **158**, A43−A46.

34.   L. J. Li and A. Manthiram, *J Mater Chem A*, 2013, **1**, 5121−5127.

35.   H. Shao, J. Wang, X. Wang, J. Zhang and C. Cao, *Electrochem Commun*, 2004, **6**, 6−9.

36.   X. Chang, J. Wang, H. Shao, J. Wang, X. Zeng, J. Zhang and C. Cao, *Acta Phys-Chim Sin*, 2008, **24**, 1620−1624.

37.   J. B. Wang, J. M. Wang, H. B. Shao, X. T. Chang, L. Wang, J. Q. Zhang and C. N. Cao, *Mater Corros*, 2009, **60**, 269−273.

38.   S. H. Yang and H. Knickle, *J Power Sources*, 2002, **112**, 162−173.

39.   T. B. Reddy, *Linden's Handbook of Batteries*, McGraw-Hill, 2011, p. 33.30−33.32.

40.   Y. G. Li, M. Gong, Y. Y. Liang, J. Feng, J. E. Kim, H. L. Wang, G. S. Hong, B. Zhang and H. J. Dai, *Nat Commun*, 2013, **4**.

41.   P. G. Bruce, S. A. Freunberger, L. J. Hardwick and J.-M. Tarascon, *Nat Mater*, 2011, **11**, 19−29.

42.   G. Cohn, A. Altberg, D. D. Macdonald and Y. Ein-Eli, *Electrochimica Acta*, 2011, **58**, 161−164.

43.   G. Cohn and Y. Ein-Eli, *J Power Sources*, 2010, **195**, 4963−4970.

44.   G. Cohn, D. Starosvetsky, R. Hagiwara, D. D. Macdonald and Y. Ein-Eli, *Electrochem Commun*, 2009, **11**, 1916−1918.

45.   Y.-C. Lu, B. M. Gallant, D. G. Kwabi, J. R. Harding, R. R. Mitchell, M. S. Whittingham and Y. Shao-Horn, *Energ Environ Sci*, 2013, **6**, 750−768.

46.   H. G. Jung, J. Hassoun, J. B. Park, Y. K. Sun and B. Scrosati, *Nat Chem*, 2012, **4**, 579−585.

47.   A. Kraytsberg and Y. Ein-Eli, *J Power Sources*, 2011, **196**, 886−893.

48.   B. Yirka, Phys.org. URL: http://phys.org/news/2013-03-phinergy-aluminum-air-battery-capable-fueling.html; Accessed on April 24, 2013.